

# The high-pressure $\alpha/\beta$ phase transition in lead sulphide (PbS)

## X-ray powder diffraction and quantum mechanical calculations

K. Knorr<sup>1</sup>, L. Ehm<sup>1</sup>, M. Hytha<sup>1 a b</sup>, B. Winkler<sup>1 c</sup>, and W. Depmeier<sup>1</sup>

Christian-Albrechts-Universität zu Kiel, Institut für Geowissenschaften, Mineralogie/Kristallographie, Olshausenstr. 40, D-24098 Kiel, Germany

October 16, 2018

**Abstract.** The high-pressure behaviour of PbS was investigated by angular dispersive X-ray powder diffraction up to pressures of 6.8 GPa. Experiments were accompanied by first principles calculations at the density functional theory level. By combining both methods reliable data for the elastic properties of rock-salt type  $\alpha$ - and high-pressure  $\beta$ -PbS could be obtained.  $\beta$ -PbS could be determined to crystallise in the CrB-type (B33), with space group  $Cmcm$ . The reversible ferro-elastic  $\alpha/\beta$  transition is of first order. It is accompanied by a large volume discontinuity of about 5% and a coexistence region of the two phases. A gliding mechanism of {001} bilayers along one of the cubic  $\langle 110 \rangle$  directions governs the phase transition which can be described in terms of group/subgroup relationships via a common subgroup, despite its reconstructive character. The quadrupling of the primitive unit cell indicates a wave vector  $(0, 0, \pi/a)$  on the  $\Delta$ -line of the Brillouin zone.

**PACS.** 91.60.Gf High-pressure behaviour – 61.50.Ks Crystallographic aspects of phase transformations; pressure effects – 77.84.Bw Elements, oxides, nitrides, borides, carbides, chalcogenides – 62.20.Dc Elasticity, elastic constants

## 1 Introduction

Among the IV-VI narrow gap semiconductors lead sulphide, PbS, has been a subject of interest during the last three decades, owing to its potential technological relevance, e.g. in long-wavelength imaging, as diode lasers [1] or thermovoltaic energy converters. Many of the experimental and theoretical investigations have been focused on the electronic structure [2,3]. Currently, PbS attracts new interest because of its importance for the understanding of the complex misfit layer compounds  $(MX)_{1+x}(TX_2)_m$  ( $M=\text{Sn, Pb, Sb, Bi, rare earth; T}=\text{Ti, V, Cr, Nb, Ta}$ ;

Send offprint requests to: K. Knorr, [knorr@min.uni-kiel.de](mailto:knorr@min.uni-kiel.de)

<sup>a</sup> Also at: Institute of Physics of the Czech Academy of Sciences, Cukrovarnicka 10, 16253 Praha 6, Czech Republic

<sup>b</sup> Present address: University of Cambridge, Cavendish Laboratory (TCM), Madingley Road, Cambridge CB3 0HE, U.K.

<sup>c</sup> Present address: Johann-Wolfgang Goethe Universität, Mineralogisches Institut, Kristallographie, Senckenberganlage 30, D 60054 Frankfurt a.M., Germany

$X=\text{S, Se; } 0.08 < x < 0.28; m=1-3$ ) [4], of which PbS can be regarded as a component structure. These composite structures are single-crystal multi-layer systems, exhibiting strong anisotropic material properties.

At ambient conditions  $\alpha$ -PbS crystallises in the rock salt structure type (B1) [5] with the lattice parameter  $a=5.9240(4)$  Å and space group  $Fm\bar{3}m$ . The elastic constants of  $\alpha$ -PbS were determined by ultrasonic velocity measurements [6]. Resistivity measurements under high pressure on several lead chalcogenides revealed the existence of a phase transition [7] which occurs in PbS at 2.2 GPa. First structural studies under high pressure were performed using X-ray film methods [8]. Later, the compression behaviour of PbS was studied by means of high-pressure energy dispersive X-ray powder diffraction (HP-EDX) up to 35 GPa [9,10,11,12,13].

The phase transition at 2.2 GPa [7] to a  $\beta$ -phase having orthorhombic symmetry was characterised as a first order transition [8,10,11]. However, the structure of this phase is still a matter of debate. Two different structure types

were proposed, viz. the GeS structure type (B16) with the space group  $Pbnm$  [7,8,12,13] and the closely related, but higher symmetric CrB structure type (B33) with the symmetry  $Cmcm$  [10,11]. A definitive decision between these two possibilities has not been possible until now on the basis of the experimental data available.

A second phase transition at about 25 GPa was detected by HP-EDX and assigned to the transformation into cubic  $\gamma$ -PbS with the CsCl (B2) type structure [10,11].

Since the equation-of-state parameters for  $\alpha$ -PbS, the symmetry of the  $\beta$  phase and its compression behaviour are hitherto unknown it was found worth reexamining the PbS system under pressure. To elucidate the structure of the intermediate  $\beta$  phase, angle dispersive X-ray powder diffraction and density functional theory (DFT) calculations were performed. Here the results of the study of the crystal structure of PbS under high pressure are presented. The mechanism of the phase transition is discussed using the symmetry relations between the space groups of the two phases.

## 2 Experimental methods

Crystals were grown by chemical vapour transport (CVT) in evacuated quartz tubes in a gradient furnace (1053 to 923 K) with stoichiometrically mixed elements as starting material and iodine as transport agent. In the low-temperature zone cube shaped crystals were obtained after several days with edge lengths up to 3 mm. The chemical composition of the crystals was checked by electron micro-probe analysis and the phase purity was studied by conventional X-ray powder diffraction.

The high-pressure experiments were performed using diamond anvil cells [14]. NaCl was used as internal standard for the pressure determination by the Decker equation-of-state [15]. Several runs were performed using a 4:1 methanol/ethanol mixture for maintaining hydrostatic conditions. The highest pressure obtained was 6.8 GPa. Angular dispersive diffraction data were collected with Mo- $K\alpha$  radiation on a MAR2000 image plate diffractometer. The geometry correction for the radial integration of the two-dimensional data and the transformation into standard one-dimensional powder patterns were performed using FIT2D [16]. Whole powder pattern fitting employing FULLPROF [17] was performed for the precise determination of the unit cell parameters.

## 3 Computational aspects

Geometry optimisations were performed for  $\alpha$ -PbS and for both proposed structure types of  $\beta$ -PbS. The *ab initio* plane-wave CASTEP code [18,19] was used which is based on the density functional theory (DFT). The exchange correlation interaction was accounted for by using the Perdew, Burke and Ernzerhof version of the generalised gradient approximation (PBE-GGA) of the exchange-correlation functional [20,21]. Ultrasoft pseudopotentials

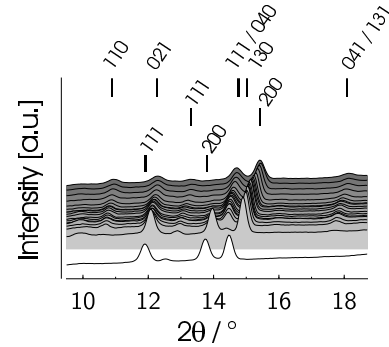


**Fig. 1.** Pressure dependence of diffraction patterns of PbS from room pressure to 6.87 GPa. The patterns are shifted with increasing pressure. Miller indices are given for  $\alpha$ -PbS (lower row), NaCl (middle) and,  $\beta$ -PbS (top row).

[22,23] with a maximum cutoff energy of the plane waves of 290 eV were used to describe the electron-ion interaction. The integration over the Brillouin zone was performed employing the Monkhorst-Pack [24] sampling scheme of reciprocal space, with a distance of  $0.04 \text{ \AA}^{-1}$  between the sampling points. All structural parameters not constrained by the space group symmetry were relaxed.

The calculation of the elastic constants is based on applying small strains to the already relaxed structure, followed by relaxation of the atomic positions. In order to avoid anharmonic effects the maximum applied distortion was about 0.2 %. Several amplitudes for each strain component were used. Elastic constants were determined from a linear fit of stress to the applied strain.

## 4 Results and discussion

Some integrated powder patterns are presented in figure 1. The onset of a phase transition was detected at 2.5 GPa by the appearance of additional reflections. The new phase could be indexed with an orthorhombic unit cell and cell parameters  $a=3.98(2) \text{ \AA}$ ,  $b=11.11(7) \text{ \AA}$  and  $c=4.16(4) \text{ \AA}$ . Coexistence of the two phases was observed up to a pressure of 6 GPa.

The powder patterns obtained above 2.5 GPa could be indexed with the same unit cell for both, B16 and B33, structure types. A structure refinement of the  $\beta$ -phase in either case turned out to be impossible because of the strong peak overlap with reflections stemming from the gasket material (Inconel steel). Thus, a discrimination between both possible structure types was not possible by the diffraction method.

### 4.1 Lattice parameters and elastic properties of $\alpha$ - and $\beta$ -PbS

The cell parameters of the orthorhombic  $\beta$ -phase are related to those of the cubic  $\alpha$ -phase by  $a_o = \sqrt{2}a_c/2$ ,  $b_o = 2a_c$ ,  $c_o = \sqrt{2}a_c/2$ , with subscripts  $o$  and  $c$  referring to



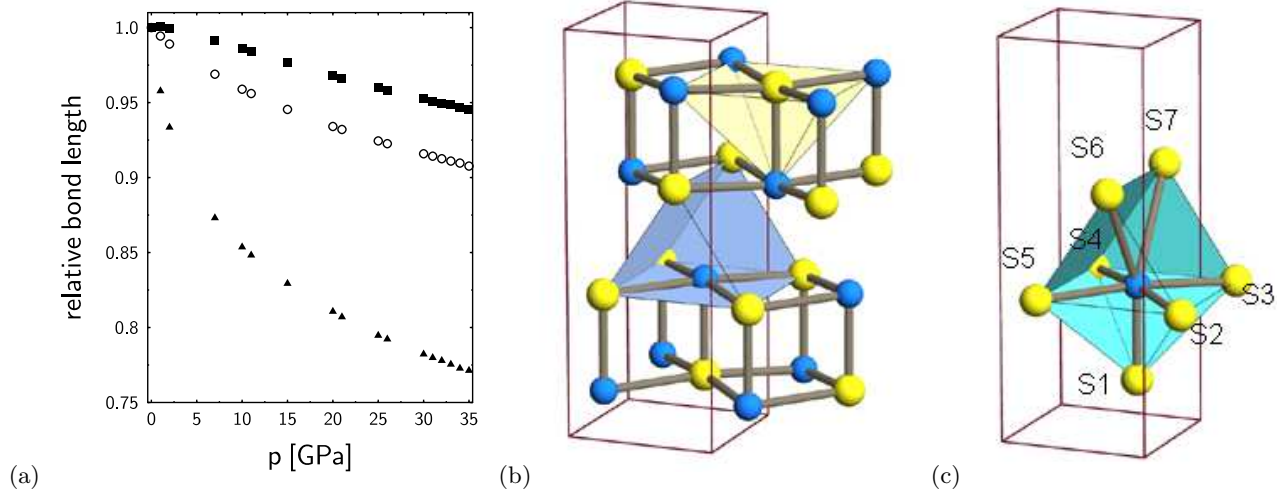


**Fig. 4.** (a) Variation of the Pb–S bond lengths in  $\beta$ -PbS from the *ab initio* calculations. In (b) and (c) coordination polyhedra and the crystal structure of  $\beta$ -PbS are drawn. Applying the labels given for the S atoms of the single-capped trigonal prism, shown in (c) the following bonds can be distinguished in graph (a): squares represent the Pb–S(1) bond pointing at the apex of the pyramid located within the bilayer in (b), circles correspond to Pb–S(2-5) bonds which constitute the base plane of the pyramid and one face of the prism, and triangles denote the Pb–S(6,7) bonds between adjacent bilayers and, being located inside the prism.

and, thus, discrimination between both possible structure types B16 and B33 for  $\beta$ -PbS. By contrast, the quantum mechanical calculations made the distinction possible, because only for the CrB-type structure (B33) convergence was achieved. The enthalpy for this phase with respect to the  $\alpha$ -phase is shown in figure 3 as a function of pressure. A transition pressure of 9.6(1) GPa for the  $\alpha/\beta$ -transformation follows from the crossover of the fitted curves. This transition pressure is higher than the experimentally determined values (onset of the transition at 2.6 GPa, this study; 2.2 GPa [7]). However, DFT-GGA calculations such as those presented here suffer from systematic ‘underbinding’ and the neglect of temperature effects. Furthermore, they refer to perfect ideal crystals. Hence, a

discrepancy of 7 GPa between observed and calculated transition pressures can be tolerated. Also, the main aim of such calculations is not to reproduce numbers, but instead provide insight into the transition mechanism, and for this purpose such calculations are well suited.

### 4.3 Compression mechanism

In  $\alpha$ -PbS the lead atoms are sixfold coordinated by sulphur atoms in a regular octahedral arrangement. The only structural parameter in the B1 structure type not constrained by the space group symmetry is the magnitude of the cell parameter. The Pb–S bond length is  $a_c/2$  and, of course, the compression mechanism results in shortening of the bond length.

No major change in the linear compressibility between cubic and orthorhombic PbS follows from the experimentally determined cell parameters (Fig. 2b). However, Pb–S bond lengths derived from the *ab initio* calculations (Fig. 4a) clearly show that the compression behaviour is anisotropic. Layered chalcogenides show a strongly anisotropic compression with the strongest compression perpendicular to the layers (e.g. TiS<sub>2</sub> [28], SnS<sub>2</sub> [29], NbS<sub>2</sub> [30]). The main compression mechanism in these compounds is narrowing of the van-der-Waals gaps, whereas the layers themselves are bonded predominately ionic. The structure of  $\beta$ -PbS can be thought of as a layer structure as well, consisting of rock salt like bilayers, stacked along the  $b$ -axis of the orthorhombic unit cell. This is shown in figure 4b where two simple coordination polyhedra can be distinguished. Within the bilayers Pb is found in a fivefold coordination for which a square pyramid is an idealised geometry. The basal pinacoid face of the square pyramid forms together with two sulphur atoms

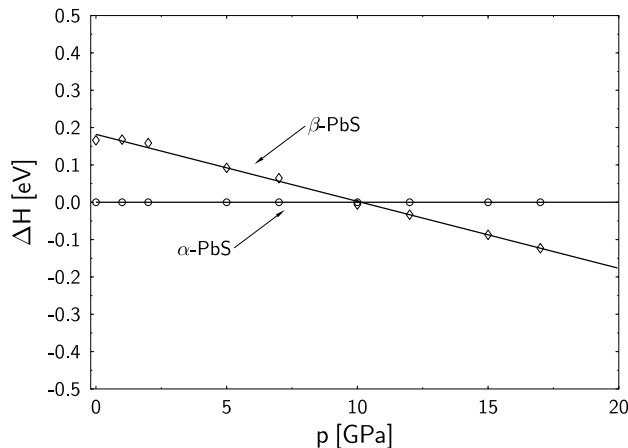


**Fig. 3.** Pressure dependence of the molar enthalpy difference between  $\alpha$ - and  $\beta$ -PbS.

**Table 2.** Geometric conditions for an ideal single-capped trigonal prism [31]. Five different edges with index  $i$  have to be distinguished occurring with frequency  $n_i$  and different edge lengths  $d_i$ . The radius of the circumsphere is  $r$  and labels are given according to Figure 4c.

| $i$ | $d_i$    | $n_i$ | label                      |
|-----|----------|-------|----------------------------|
| 1   | $1.277r$ | 4     | S1–S2,3,4,5                |
| 2   | $1.297r$ | 2     | S2–S3, S4–S5               |
| 3   | $1.233r$ | 4     | S2–S6, S5–S6, S3–S7, S4–S7 |
| 4   | $1.195r$ | 1     | S6–S7                      |
| 5   | $1.478r$ | 2     | S2–S5, S3–S4               |

from the next bilayer an almost trigonal prism. Figure 4a shows the strongest compression for this particular coordination polyhedron. The Pb–S(6,7) bonds connect the layers. The two different bonds within the bilayers are less compressible. While the pyramids deform almost isotropically, the main compression mechanism is a distortion of the trigonal prism, due to a change of the Pb–S(6,7) bond lengths. This mechanism effectively influences the length of the  $b$ -axis. Changes in the  $a$  and  $c$  axes are related to lateral distortions within the bilayers, i.e. changes of the Pb–S(2-5) bond lengths, and of the angles between them.

Admittedly, a description of the coordination in  $\beta$ -PbS by two different polyhedra is not fully appropriate since this approach doesn't account for the increase of the coordination number with pressure. Alternatively, the coordination of the lead atoms can be described as sevenfold with the geometry of a single-capped trigonal prism [31]. The capped trigonal prism in  $\beta$ -PbS is shown in Figure 4c. The ideal geometry of a single-capped trigonal prism requires that all apices are located on the surface of a sphere and the edges  $d_i$  fulfil the conditions given in table 2 [31]. The deviation of this coordination polyhedron from ideal can be quantified by applying e.g. the Pinsky and Avnir continuous-symmetry-measure (CSM) [32]. Here a simplified CSM formulation was used.

From the five different edges  $d_i$  radii  $r_i$  were determined according to table 2 and from the weighted average radius

$$\bar{r}_w = \frac{\sum_{i=1}^5 n_i r_i}{\sum_{i=1}^5 n_i}, \quad (1)$$

the edge lengths of the corresponding ideal polyhedron  $d_i^*$  could be calculated. The average distortion measure ADM is then given by

$$\text{ADM} = \frac{\sum_{i=1}^5 n_i (d_i - d_i^*)^2}{\sum_{i=1}^5 (n_i d_i^*)^2} \times 100 \quad (2)$$

and the mean edge length distortion is

$$\bar{\Delta}_d = \sqrt{\frac{\sum_{i=1}^5 n_i (d_i - d_i^*)^2}{\sum_{i=1}^5 n_i}}. \quad (3)$$

The ADM is normalised with respect to the edge lengths of the ideal polyhedron in order to compensate for the effect

**Table 3.** Distortion measures of the single-capped trigonal prism in  $\beta$ -PbS at selected pressures, obtained from DFT calculations.

| p [GPa] | $\delta_y$ [Å] | $\bar{r}_w$ [Å] | ADM   | $\bar{\Delta}_d$ [Å] |
|---------|----------------|-----------------|-------|----------------------|
| 0       | .3594          | 3.201           | .0289 | .0702                |
| 2       | .2149          | 3.117           | .016  | .0512                |
| 7       | .1005          | 3.019           | .0114 | .0416                |
| 10      | .0692          | 2.979           | .0111 | .0405                |
| 15      | .0355          | 2.928           | .0102 | .0382                |
| 21      | .0095          | 2.879           | .0105 | .0381                |
| 25      | .0099          | 2.852           | .0099 | .0367                |

of the compression. Hence, it is a dimensionless number. The compression of the coordination polyhedron is represented by the change of of the circumsphere's radius  $\bar{r}_w$  with pressure. The mean edge length distortion  $\bar{\Delta}_d$  is a measure of the variance of the edges. The resulting values for selected pressures are given in Table 3. At low pressures the conformation of the coordination polyhedron deviates most strongly from that of an ideal single-capped trigonal prism [31] (ADM=0). With increasing pressure ADM and  $\bar{\Delta}_d$  indicate increasing regularity of the coordination polyhedron. Above approximately 10 GPa some residual deformation remains virtually constant. The position of the central lead atom does not coincide with the conjoint centroid of the seven sulphur ligands (the difference  $\delta_y$  is along the orthorhombic  $b$  direction and given in table 3). With increasing pressure the position of Pb tends towards that of the sulphur's centroid. A similar behaviour has recently been reported for  $\alpha$ -PbF<sub>2</sub> [33], where Pb is elevenfold coordinated by F in a tri-capped trigonal prism.

#### 4.4 Characterisation of the $\alpha/\beta$ phase transition

Coexistence of the two phases between 2.5 and 6 GPa was observed. Since the peak profile remained sharp throughout the whole pressure range covered by the experiment, pressure inhomogeneities can be excluded as the origin of this phase coexistence. Instead, it reflects the first order character of the transition (e.g. [10,11]). This is further supported by the observed discontinuity in the molar volume of 4.7 % at the phase transition.

The transition is reconstructive. This is justified by i) the change of the coordination number from six to seven, and ii.) because there is no direct group/subgroup relationship between the two space groups  $Fm\bar{3}m$  and  $Cmcm$ . Figure 5 shows the symmetry relations in terms of *klassen-gleiche* (index  $k$ ) and *translationengleiche* (index  $t$ ) subgroups together with the changes of the unit cell dimensions. The crucial step here is the transition to space group  $Pbnm$  realised by a displacement  $0 < \Delta a < 1/2$  of every second (001)-bilayer along the orthorhombic  $a$ -, i.e. cubic  $\langle 1\bar{1}0 \rangle$ , direction. The space group  $Cmcm$  is obtained as a limit state, when  $\Delta a$  takes the value of  $1/2$ . It is interesting to note that the displacement is the same as for the preferential glide system  $\langle 1\bar{1}0 \rangle \{001\}$  of NaCl. In the  $\langle 1\bar{1}0 \rangle$

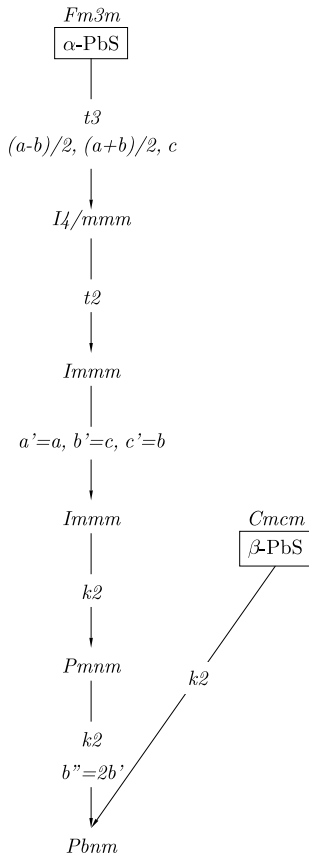


**Fig. 5.** Group/subgroup diagram for the  $\alpha/\beta$  phase transition in PbS, showing a possible transition pathway from space group  $Fm\bar{3}m$  to  $Cmc$  via the common subgroup  $Pbnm$ .

directions easy displacements of  $\{001\}$  layers are possible because movement of the ions occurs without having contact of equally charged ions.

The  $\alpha/\beta$  transition in PbS is accompanied by a quadrupling of the unit cell. The wave vector of the transition is  $(0, 0, \pi/a)$  in the midpoint of the  $\Delta$ -line connecting the  $\Gamma$ -point at the zone centre with the  $X$ -point on the boundary of the Brillouin zone of the cubic face-centred lattice.

## 5 Summary and conclusion

The elastic behaviour of  $\alpha$ - and  $\beta$ -PbS was measured up to 6.8 GPa. Bulk moduli, elastic constants and linear compressibilities were determined by DFT calculations and compared to experiment. The symmetry of  $\beta$ -PbS was found to be  $Cmc$ . The differences in the compression behaviour between  $\alpha$  and  $\beta$ -PbS can be understood on the basis of the different crystal structures and consequently, different compression mechanisms. PbS bilayers as found in the  $\beta$ -phase occur as MX subsystem of the chalcogenide misfit layer compounds [4]. Structural investigations under high pressure are not known for the misfit layer compounds. Therefore, our findings for the compression mechanism in  $\beta$ -PbS may serve at least as model for

the MX subsystem in misfit layer compounds. Of course, for a better understanding of the elastic properties of the MX-TX<sub>2</sub> multi-layer systems further investigations are required.

## Acknowledgement

This research was performed in the framework of the Kieler Forschergruppe "Wachstum und Grenzflächeneigenschaften von Sulfid- und Selenid-Schichtstrukturen" funded by the German Science Foundation DFG (De412/21-1).

## References

1. J. Philipps, T. Töpfer, H. Ebendorff-Heidepriem, D. Ehrt, R. Sauerbrey, N. Borrelli, Applied Physics B **72** 175 (2001)
2. A. Santoni, G. Paolucci, G. Santoro, K. Prince, N. Christensen, J. Phys. Cond. Matter **4** (1992)
3. S.-H. Wei, A. Zunger, Phys. Rev. B **55** 130605 (1997)
4. J. Rouxel, A. Meerschaut, G. Wieggers, J. Alloys Comp. **229** 144 (1995)
5. B. Wasserstein, Am. Miner. **36** 102 (1951)
6. V. Padaki, S. Lakshimikumar, S. Subramanyam, E. Gopal, Pramana **17** 25 (1981)
7. G. Samara, H. Drickamer, J. Chem. Phys. **37** 1159 (1962)
8. I. Wakabayashi, H. Kobayashi, S. Minomura, J. Phy. Soc. Jpn. **25** 227 (1968)
9. G. Peresada, E. Ponyatovskii, Z. Sokolovskaya, Phys. stat. sol. **35** K177 (1976)
10. T. Chattopadhyay, A. Werner, H. von Schnering, Mat. Res. Symp. Proc. **22** 93 (1984)
11. T. Chattopadhyay, H. von Schnering, W. Grosshans, W. Holzapfel, Physica B **139** & **140** 356 (1986)
12. S. Quadri, J. Yang, B. Ratna, E. Skelton, J. Hu, Appl. Phys. Lett. **69** 2205 (1996)
13. J. Jiang, L. Gerward, R. Secco, D. Frost, J. Olson, J. Trukenbrodt, J. Appl. Phys. **87** 2658 (2000)
14. L. Merrill, W. Bassett, Rev. Sci. Instrum. **45** 290 (1974)
15. D. Decker, J. Appl. Phys. **42** 3239 (1971)
16. A. Hammersley, S. Svensson, M. Hanfland, A. Fitch, D. Häusermann, High Pressure Research **14** 235 (1996)
17. J. Rodriguez-Carvajal, Program FULLPROF (Version 3.1c) for Rietveld, Profile Matching & Integrated Intensity Refinement of X-ray and/or Neutron Data, Laboratoire Leon Brillouin, CEN Saclay (1993)
18. M. Payne, M. Teter, D. Allan, T. Arias, J. Joannopoulos, Rev. Mod. Phys. **64** 1045 (1992)
19. V. Milman, B. Winkler, J. White, C. Pickard, M. Payne, E. Akhmatkaya, R. Nobes, Int. J. Quant. Chem. **77** 895 (2000)
20. J. Perdew, J. Chevary, S. Vosko, K. Jackson, M. Pederson, D. Singh, C. Fiolhais, Phys. Rev. B **46** 6671 (1992)
21. J. White, D. Bird, Phys. Rev. B **50** 4954 (1994)
22. D. Vanderbilt, Phys. Rev. B **41** 7892 (1990)
23. G. Kresse, J. Hafner, J. Phys. Cond. Matter **6** 8245 (1994)
24. H. Monkhorst, J. Pack, Phys. Rev. B **13** 5188 (1976)
25. F. Birch, J. Geophys. Res. **83** 1257 (1978)
26. P. Paufler, *Physikalische Kristallographie* (Akademie-Verlag, Berlin, 1986)

27. R. J. Angel, *High-Temperature and High-Pressure Crystal Chemistry*, volume 41 of *Reviews in Mineralogy and Geochemistry*, chapter Equations of State, pp. 36–59 (Mineralogical Society of America, Washington, DC, 2000)
28. D. R. Allan, A. A. Kelsey, S. J. Clarek, R. J. Angel, G. J. Ackland, *Physical Review* **B57** 5106 (1998)
29. K. Knorr, L. Ehm, M. Hytha, B. Winkler, W. Depmeier, *Phys. Stat. Sol. b* **223** 435 (2001)
30. L. Ehm, K. Knorr, W. Depmeier, *Z. Kristallogr. p.* in print (2002), e-print arXiv:cond-mat/0209232
31. D. L. Kepert, *Inorganic Stereochemistry*, volume 6 of *Inorganic Chemistry Concepts* (Springer-Verlag, Berlin, Heidelberg, New York, 1982)
32. M. Pinsky, D. Avnir, *Inorg. Chem.* **37** 5575 (1998)
33. L. Ehm, K. Knorr, F. Mädler, H. Voigtländer, E. Busetto, A. Cassetta, A. Lausi, B. Winkler, *J. Phys. Chem. Sol.* (2002), submitted; e-print arXiv:cond-mat/0209082